SUBMERGED ARC WELDING EFFECT OF WELDING SPEED ON PRESSURE VESSEL STEEL P355N TENSILE STRENGTH AND MICROSTRUCTURE

Bogdan-Dorel CIOROAGĂ [1*], Ana Virginia SOCALICI [2], Vasile George CIOATĂ [3], Emanoil LINUL [4], Iosif HULKA [5]

This research investigates the effect of welding speed on P355N pressure vessels using submerged arc welding to optimize industrial welding processes, such as for liquid-transporting railway wagons. Key objectives include enhancing productivity while maintaining tensile strength. Experiments evaluated welding speeds of 25, 50, 75, 100, and 125 cm/min, analyzing tensile strength, microstructure (SEM), and geometric dimensions of welded joints. Results aim to guide welding operators in adjusting welding speed to achieve improved efficiency without compromising joint quality.

Keywords: welding, strees, microstructure, speed, optimization.

1. Introduction

Submerged Arc Welding (SAW) is widely used in pressure vessel fabrication for its high-quality welds, deep penetration, and minimal contamination. P355N steel, a normalized pressure vessel steel, is commonly employed in pressure vessels and boilers due to its mechanical properties and weldability.

Understanding the impact of welding speed on mechanical properties and microstructure is crucial for optimizing welding processes and ensuring the structural integrity and performance of welded components.Previous studies have extensively explored various aspects of SAW on P355N steel, highlighting the impact of different welding parameters on the weld quality, microstructure, and mechanical properties. The specific influence of the welding speed consists in affecting heat input which directly affects the rate of deposition and penetration of

* Corresponding author
[1] Politehnica University Timişoara, Faculty of Engineering in Hunedoara, Romania, bogdan.cioroaga@student.upt.ro
[2] Politehnica University Timişoara, Faculty of Engineering in Hunedoara, Romania, virginia.socalici@fih.upt.ro
[3] Politehnica University Timişoara, Faculty of Engineering in Hunedoara, Romania, vasile.cioata@fih.upt.ro
[4] Politehnica University Timişoara, Faculty of Mechanical Engineering, Romania, emanoil.linul@upt.ro
[5] Politehnica University Timişoara, Research Institute for Renewable Energy, Romania, iosif.hulka@upt.ro

the filler material and as an economic parameter productivity is directly affected, warrants a more detailed investigation to refine our understanding and application in industrial contexts.

Research has established the impact of welding parameters on the mechanical properties and microstructure of P355N steel in SAW. Li, Yang, and Jiang (2017) [1] highlighted the role of heat input, showing that welding speed variations significantly influence microstructure and mechanical properties.

Wang, Li, and Liu (2018) [2] confirmed that precise welding speed control optimizes grain size and phase distribution, enhancing mechanical performance. Sharma and Gupta (2020) [3] further demonstrated that welding speed affects hardness and tensile strength, emphasizing the need for optimization.

Li et al. (2021) [4] linked welding speed to cooling rate, influencing microstructural phase formation. Wu, Chen, and Zhang (2023) [5] conducted detailed microstructural characterization, identifying mechanisms driving mechanical property changes.

The latest study by Jain and Patel (2024) [6] examined optimal welding speed ranges, demonstrating that proper selection enhances weld quality and mechanical properties.

Despite extensive research, a gap remains in the precise quantification of welding speed effects on P355N steel's mechanical properties and microstructure across varied conditions. Most studies focus on narrow speed ranges or individual mechanical properties, lacking an integrated analysis of weld quality factors like toughness, hardness, tensile strength, and microstructural characterization.This study analyzes the effect of welding speed on the microstructure and mechanical properties of P355N steel welded via SAW, focusing on tensile strength, hardness, and toughness. A key objective is to correlate welding speed with microstructural evolution and mechanical performance, identifying optimal speed ranges for railway pressure vessel wagons.

Utilizing advanced characterization techniques, the research fills existing knowledge gaps by providing guidelines for selecting welding parameters, enhancing weld reliability and performance in pressure vessel manufacturing.

This study contributes to welding metallurgy by offering a detailed dataset for future research and industrial applications, with practical recommendations to optimize the SAW process for improved weld quality and mechanical performance.

2. Materials and Methods

2.1. Materials

To conduct the experiments, six welded joints were produced using submerged arc welding technology, each with a length of 300 mm. From each welded joint, three tensile test specimens were extracted, and a metallographic sample was obtained from each of the six welding regimes. The base material used

for the welded joints was a 6 mm-thick laminated steel sheet, specifically P355N steel, designed for pressure vessels (as specified in EN 10027-1:2005 and corresponding to the standard SR EN 10216-3:2003) [7,8].

The filler material employed was an OK Autrod 12.24 electrode wire (as named by its manufacturer, ESAB, Hanover, PA, USA), a molybdenum-alloyed steel with a copper coating, intended specifically for submerged arc welding of pressure vessel steel.

The chemical composition of the base material (P355N) was as follows (maximum values): carbon, 0.2%; silicon, 0.5%; manganese, 1.7%; phosphorus, 0.025%; sulfur, 0.02%; aluminum, 0.02%; chromium, 0.3%; copper, 0.3%; molybdenum, 0.08%; niobium, 0.05%; nickel, 0.5%; titanium, 0.04%; and vanadium, 0.1% [8].

The chemical composition of the filler material (OK Autrod 12.24) was as follows (maximum values): carbon, 0.12%; silicon, 0.2%; manganese, 1.2%; phosphorus, 0.02%; sulfur, 0.02%; and molybdenum, 0.6% [9].

The OK Flux 10.72 (ESAB, Pennsylvania, USA) is a powder flux with a grain size of 0.315 to 2 mm, providing a protective environment that shields the weld pool from atmospheric contamination. It also enhances operator safety by blocking light radiation and preventing gas escape from the molten bath.

Additionally, the flux slows cooling and aids in alloying the weld pool, preserving key elements that might otherwise be lost [10,11]. The base and filler materials have similar alloying elements, particularly carbon, classifying them as hypoeutectoid steels. Under normal cooling, they form ferritic and pearlitic structures, whereas accelerated cooling may result in martensitic and bainitic microstructures in the weld joint area.

2.2. Manufacturing Process

2.1.1. Manufacturing of Welding Joints

The semi-automatic welding machine ensured constant welding parameters and consisted of a mobile beam, electrode holder torch, wire drum, and flux management system. The LAF 613-ESAB power source and PEK-ESAB control unit controlled arc parameters and travel speed. The beam moved vertically for torch positioning and horizontally for longitudinal joints.

Welded samples were produced by butt-welding two 6×125×300 mm plates with a 1 mm gap, using a type I joint. The plates were guillotine cut, ground to remove oxides, and secured with tack welds before clamping to the worktable. Welding was performed in a single pass, horizontal position, with a 25 mm thick flux layer applied [12].

The welding parameters remained constant throughout the experiments.

- Welding voltage: 33 V
- Welding current: 480 A

- Welding speed: 60 cm/min
- Electrode tilt angle: 90 degrees

In addition to the standard welding regime, which used the above parameters, five other welding regimes with varying welding speed (25 cm/min, 50 cm/min, 75 cm/min, 100 cm/min, and 125 cm/min) were also tested. Fig. 1 shows the resulting welded samples after these procedures.

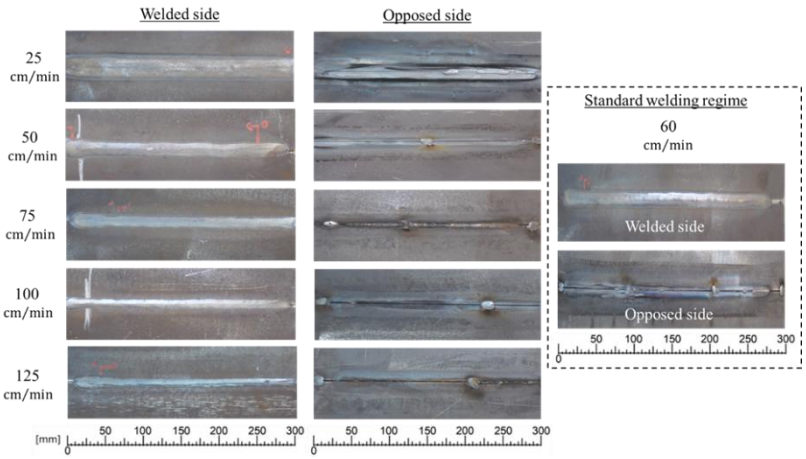

Fig. 1. Samples welded using SAW with different stages of welding speed

For each set of samples, a ceramic backing bar with a convex profile was used to support the molten material at the root of the joint, preventing it from completely leaking through. This method is commonly applied in the industrial production of railway tank wagons. As shown in Fig. 2, the top side of the samples represents the welded surface, while the bottom side is the opposite face. Welding currents below 500 A led to incomplete joint penetration, preventing the filler material from fully extending. In contrast, currents above 500 A caused a pronounced heat-affected zone (HAZ), visible as a blue-green coloration on the bottom side [13].

2.1.2. Manufacturing of Tensile Specimen

From the welded samples, three specimens were extracted for transverse tensile testing. The extraction of tensile test specimens was performed according to the standard "Destructive Tests on Welds in Metallic Materials - Transverse Tensile Test BS EN 895:1995" [14]. The specimens were initially cut using a guillotine, and the final shape was achieved by milling, employing oil cooling and a light cutting process to avoid thermal effects on the specimen material. Fig. 2 displays the geometry and dimensions of the tensile test specimens.

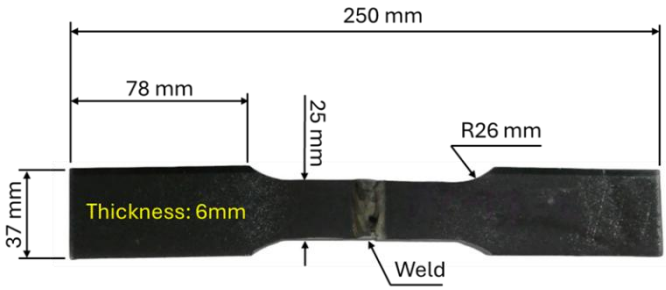

Fig. 2. Tensile test specimen dimensions

2.1.3. Manufacturing of metallographic samples

Samples were collected from specimens welded at standard conditions and 25, 75, and 125 cm/min. Metallographic samples for microstructure analysis (Fig. 5) were examined using a scanning electron microscope (SEM).

The sample preparation involved cutting with a saw under continuous oil cooling to prevent thermal alterations. The samples were then embedded in resin tablets with parallel flat surfaces and polished using abrasive cloths (280–4000 grit) to a mirror finish. Finally, the etched surface was treated with Nital reagent to reveal grain boundaries and the microstructure of the welded joint [15,16,17].

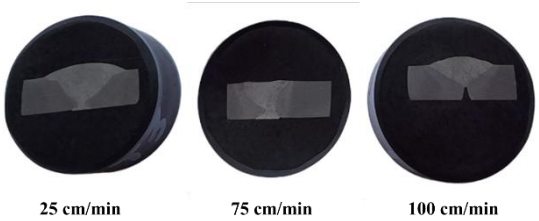

Fig. 3. Samples for microstructure analysis

2.3. Experimental Setup

2.3.1. Visual and dimensional evaluation of welded seams

The data obtained from direct measurements of the height (H) and width (W) dimensions of the welded seam consist of average values, derived from four measurements on each welded sample: two taken at the ends of the weld and one in the middle of the sample. These measurements were conducted using Lumytools LT15240 digital calipers, 150 mm, with a precision of 0.02 mm.

2.3.2. Tensile Test

The tensile test specimens were secured in a universal testing machine (A009 TC100, 100 kN capacity), featuring fixed and mobile clamps. The mobile clamp applied tensile force until fracture, with the force and movement recorded.

The collected data was processed into stress-strain curves for each welding regime, providing key resistance characteristics, including maximum force, stress

before fracture, strain at various stress levels, yield tensile stress, and strain energy before fracture [18].

The tensile load was applied quasi-statically at 50 MPa/s. A transverse force was applied to the welded joint, focusing on the middle section of the test specimen within the fracture zone. The test concluded when the specimen fractured, with possible fracture paths occurring either through the base material or the weld seam. All tests were conducted at room temperature.

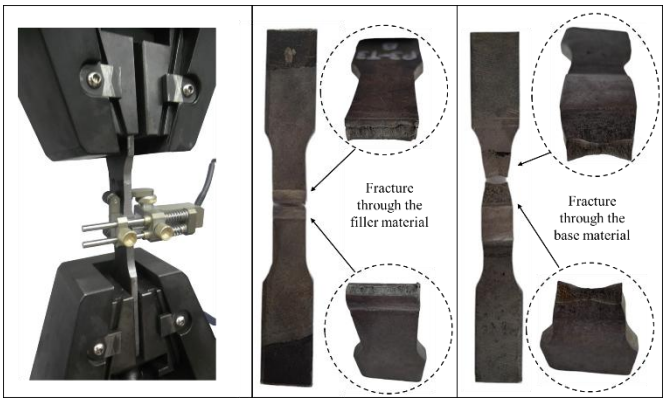

Fig. 4. Tensile teste machine and broken test smples

2.3.3. Microstructure

The specimens were prepared by cutting them to appropriate sizes, with cooling oil used to prevent thermal effects during cutting. After cutting, the specimens were embedded in resin and polished with several grades of abrasive cloth until a smooth, flat surface was achieved.

The final test piece was circular with two parallel faces, one of which was the polished surface for SEM investigations. Before testing, the samples were etched with a reagent to highlight the heat-affected zone (HAZ).

The microstructural examination was performed using a scanning electron microscope (Quanta FEG 250, FEI, Hillsboro, OR, USA) equipped with a secondary electron detector (SE) operating.

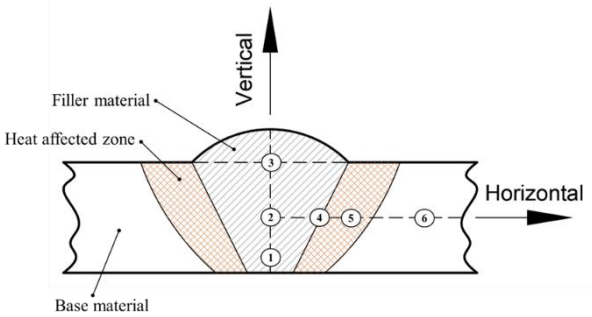

Fig. 5. Microstructure probing scheme in cross-section of the welded joint

3. Results and Discussion

3.1. Dimensional Analysis of Welds

Fig. 6 shows the correlation between welding speed and weld seam dimensions. As welding speed increases, both weld height and width decrease due to lower heat input and reduced molten metal deposition.

At lower speeds (25–50 cm/min), wider and taller weld seams form due to higher heat input. Specifically, at 25 cm/min, weld width is 35% larger, and height is 30% greater than at 125 cm/min.

At higher speeds (100–125 cm/min), welds become thinner and narrower, with 125 cm/min weld width reduced by 40% and height by 35% compared to 25 cm/min, indicating limited filler material deposition.

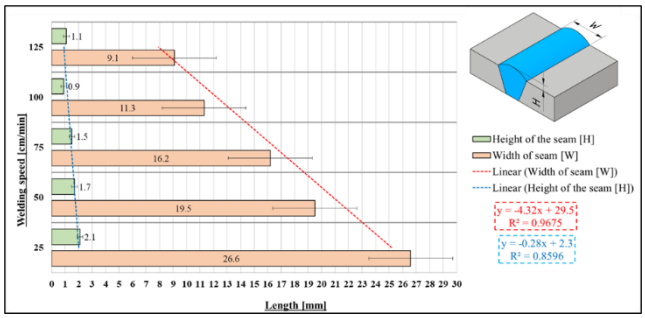

Fig. 6. Corelation between welding seam dimensions and welding speed

This trend aligns with established findings in welding studies, which indicate that slower welding speeds increase heat input, resulting in larger, more substantial welds, while higher speeds reduce the weld dimensions.

The optimal geometry for the weld seam, where adequate penetration is achieved without excessive material deposition, appears to be at a welding speed of approximately 75 cm/min. This speed strikes a balance in heat input, ensuring complete joint penetration while avoiding overly thick or wide seams, which could otherwise lead to material waste and potential weaknesses in the weld joint.

3.2. Tensile Results

The stress-strain curves in Fig. 7 illustrate the impact of welding speed on mechanical properties. At 25 cm/min, the weld exhibits the highest stress resistance (500 MPa) and strain before failure (21%), indicating higher tensile strength and ductility due to increased heat input and slower cooling. In contrast, at 125 cm/min, stress resistance drops to 300 MPa with reduced strain, showing a decline in mechanical performance. The standard speed of 60 cm/min offers a balance between strength (325 MPa) and ductility, making it suitable for applications requiring both mechanical integrity and productivity.

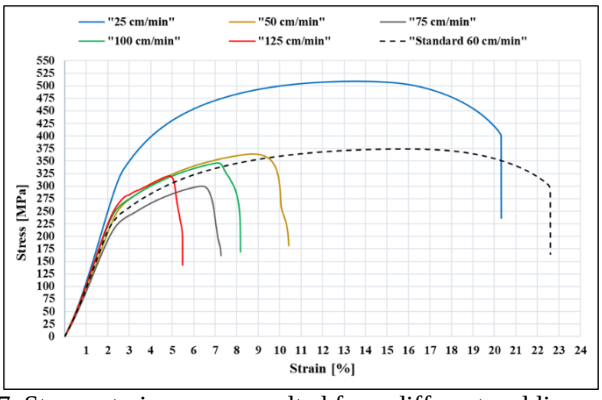

Fig. 7. Stress–strain curves resulted from different welding speeds

The data analysis highlights the impact of welding speed on stress-strain behavior and mechanical properties. The bar chart in Fig. 8 shows that at 25 cm/min, the weld achieves the highest maximum stress (498 MPa) and yield tensile stress (220 MPa), offering superior strength but lower productivity. In contrast, at 100 cm/min and 125 cm/min, both maximum and breaking stress decrease, confirming that higher welding speeds weaken joints. The standard speed of 60 cm/min provides a maximum stress of 368.50 MPa and yield tensile stress of 235.54 MPa, balancing mechanical performance and industrial efficiency, making it suitable for pressure vessel applications.

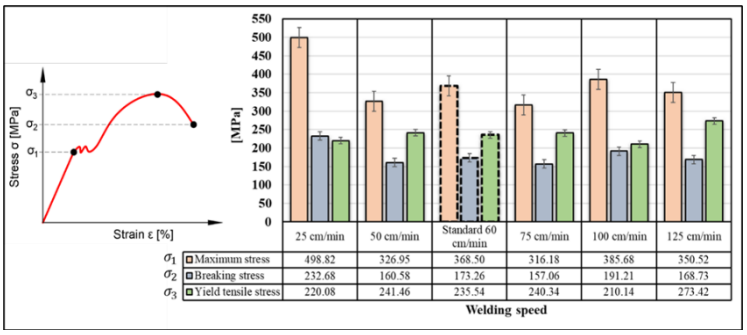

Fig. 8. Stress results from tensile tests on welding specimens.

The strain results presented in Fig. 9 highlight how welding speed affects the deformation behavior of the joints. At 25 cm/min, the strain at breaking point is 15.41%, showing high ductility. Conversely, at 125 cm/min, the strain at breaking decreases significantly to 5.98%, indicating a more brittle failure. The standard speed of 60 cm/min maintains a relatively high strain of 15.71%, indicating that the joint retains significant ductility while benefiting from a higher welding speed. These results confirm that lower welding speeds result in more ductile welds, while higher speeds, due to the rapid cooling of the weld pool, produce more brittle joints.

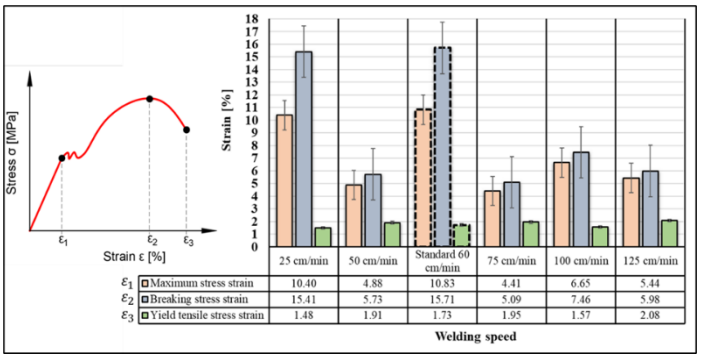

		25 cm/min	50 cm/min	Standard 60 cm/min	75 cm/min	100 cm/min	125 cm/min
ε_1	Maximum stress strain	10.40	4.88	10.83	4.41	6.65	5.44
ε_2	Breaking stress strain	15.41	5.73	15.71	5.09	7.46	5.98
ε_3	Yield tensile stress strain	1.48	1.91	1.73	1.95	1.57	2.08

Fig. 9. Strain results from tensile tests on welding specimens.

Higher welding speeds result in brittle welds with reduced ductility. A speed of 60 cm/min strikes a good balance, providing adequate ductility and avoiding the significant brittleness seen at higher speeds.

The optimal welding speed for SAW of P355N steel is 60 cm/min, balancing mechanical performance and productivity. This speed provides good tensile strength, stress resistance, and ductility, while maintaining higher production rates.

Lower speeds (25 cm/min) improve mechanical properties but reduce productivity, whereas higher speeds (100+ cm/min) weaken weld integrity and should be avoided in critical applications like pressure vessels.

Thus, 60 cm/min is ideal for industrial applications, ensuring mechanical reliability and production efficiency while meeting welding standards.

3.3. Microstructure Analysis

The SEM images in Fig. 10 illustrate microstructural variations with welding speed. At 25 cm/min, large, well-defined grains form due to slow cooling, enhancing ductility. Higher magnification (x20000) reveals clear grain boundaries with minimal defects, indicating that lower welding speeds foster a stable, defect-free microstructure, improving mechanical stability.

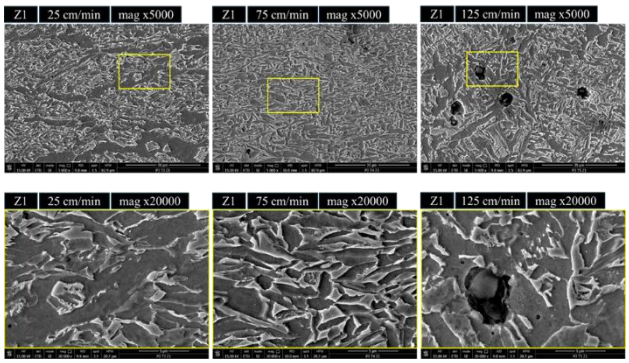

Fig. 10. Metallographic structure inspection results using SEM for zone 1

At 75 cm/min (Fig. 11), grains become smaller and slightly elongated due to faster cooling, forming a finer, more fragmented structure that enhances hardness but slightly reduces ductility. At 125 cm/min, SEM images in Fig. 12 reveal porosity defects and incomplete fusion, as rapid cooling prevents full grain boundary development, leading to shrinkage cavities that weaken mechanical properties. Zone 2 follows a similar trend (Fig. 13), where 25 cm/min produces coarse, equiaxed grains with minimal defects, promoting better ductility and toughness.

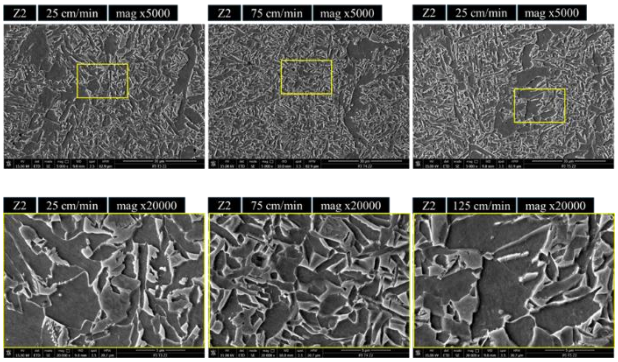

Fig. 11. Metallographic structure inspection results using SEM for zone 2

At 75 cm/min (Fig. 12, Zone 3), the microstructure becomes finer and more columnar, with sharper grain boundaries visible at higher magnifications. However, microstructural discontinuities may act as stress concentrators, potentially leading to failure under mechanical load. At 125 cm/min, SEM images at x5000 magnification reveal porosity and cracks, indicating rapid solidification and thermal stress, with more pronounced voids at higher magnification due to incomplete grain boundary formation. In Zone 3 (Fig. 12, x5000), a large cavity appears at 25 cm/min, likely caused by thermal stress or shrinkage, suggesting that even slower speeds can introduce localized imperfections.

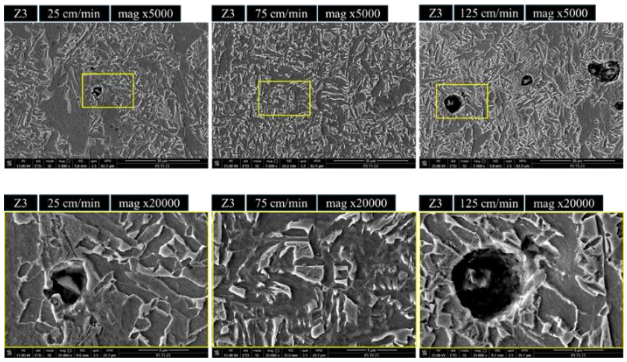

Fig. 12. Metallographic structure inspection results using SEM for zone 3

At 75 cm/min (Fig. 13, Zone 4), the microstructure becomes finer and more elongated, following the thermal gradient due to faster cooling rates. At x20000 magnification, the grain structure is well-defined, but minor porosity and microstructural fragmentation appear, which could act as nucleation sites for failure under mechanical stress.

At 125 cm/min, SEM images at lower magnification reveal significant porosity and cracks, while at higher magnification, interconnected voids and fragmented grain boundaries become more pronounced, indicating rapid solidification defects that weaken mechanical integrity.

In Fig. 13, Zone 4, at 25 cm/min, the microstructure remains coarse and well-developed, with few minor cavities resulting from thermal gradients or shrinkage, but these defects are not substantial enough to compromise overall stability.

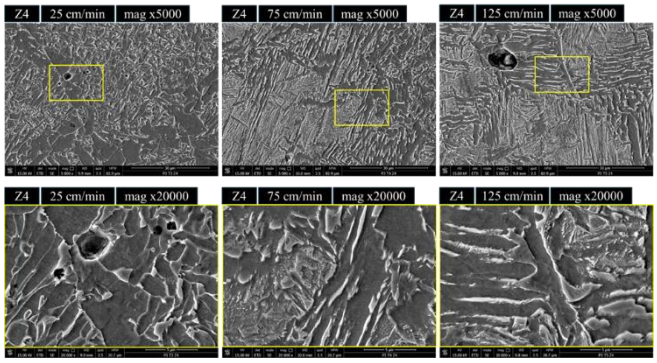

Fig. 13. Metallographic structure inspection results using SEM for zone 4

At 75 cm/min (Fig. 14, Zone 5), the microstructure becomes finer and more directional, with elongated grains forming due to faster cooling. This columnar structure enhances hardness while retaining some toughness. At higher magnification (x20000), well-defined grain boundaries are observed, though minor porosity appears, likely from incomplete fusion or trapped gas, which could impact fatigue resistance.

At 125 cm/min, SEM images at x5000 and x20000 reveal increased porosity and structural fragmentation, with large, interconnected voids and angular grain boundaries, indicating rapid solidification defects. These imperfections reduce tensile strength and increase brittleness, especially under cyclic loading conditions.

In Fig. 14, Zone 5, at 25 cm/min, the microstructure at x5000 magnification shows large, equiaxed grains with clear boundaries, characteristic of slow cooling that allows atomic diffusion and grain growth. At x20000 magnification, smooth and continuous grain boundaries are visible, with no major structural defects, suggesting that this welding speed provides enhanced ductility and mechanical uniformity.

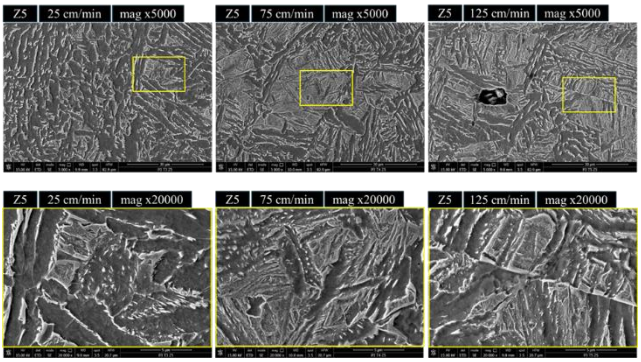

Fig. 14. Metallographic structure inspection results using SEM for zone 5

t 75 cm/min (Fig. 15, Zone 6), the microstructure becomes finer and more directional, with elongated grains forming a columnar structure due to faster cooling. At x5000 magnification, the material appears more fragmented, enhancing hardness at the cost of some ductility. At x20000 magnification, minor porosity and microcracks emerge, indicating that faster cooling introduces imperfections that may act as stress concentrators under mechanical load.

At 125 cm/min, SEM images at x5000 magnification reveal a large pore, suggesting incomplete fusion and rapid solidification defects, including shrinkage cavities. At x20000 magnification, microvoids and distorted grain boundaries are more pronounced, indicating high brittleness due to rapid cooling preventing full atomic bonding. While fine grains improve hardness, porosity and cracks severely weaken mechanical integrity.

In Fig. 15, Zone 6, SEM analysis of the base material P355N shows an unaltered ferritic-pearlitic steel structure, with clearly defined grain boundaries at x5000 magnification. The ferritic phase appears brighter, while pearlitic regions, composed of ferrite and cementite layers, appear darker and more complex, confirming the material's stability before welding-induced changes.

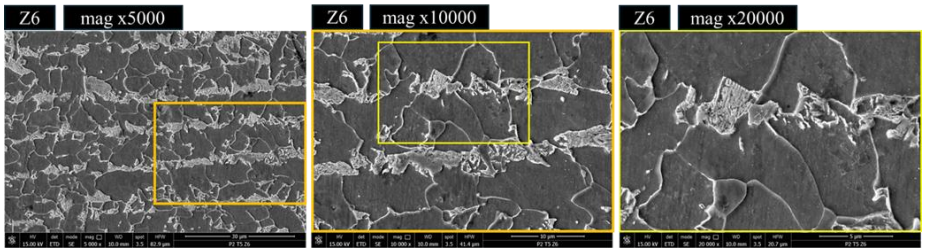

Fig. 15**.** Metallographic structure inspection results using SEM for zone 6

At 10000x magnification (Fig. 15, Zone 6), the pearlitic colonies display fine structural details, distinguishing ferrite and cementite interactions, crucial for mechanical toughness and deformation resistance.

At 20000x magnification, the ferritic-pearlitic phases appear refined, confirming a normalized steel structure with a balance of ductility and strength. The absence of thermal degradation or grain coarsening suggests that this zone remains unaffected by welding, reinforcing its suitability for high-pressure applications like pressure vessels.

The SEM analysis highlights that welding speed significantly alters P355N steel's microstructure. At 25 cm/min, large equiaxed grains form due to slow cooling, resulting in high ductility and mechanical stability. At 75 cm/min, grains become finer and more elongated, increasing hardness but slightly reducing ductility, with minor porosity acting as stress concentrators.

At 125 cm/min, rapid cooling induces porosity, cracks, and incomplete fusion, leading to a fragmented microstructure and higher brittleness, increasing failure risk under dynamic loading. The findings confirm that lower welding speeds produce a stable, ductile microstructure, while higher speeds introduce defects that degrade mechanical performance.

4. Conclusions

This study examined the effect of welding speed on the mechanical and microstructural properties of P355N steel in pressure vessel construction, aiming to optimize the SAW process. The findings confirm that welding speed significantly impacts microstructure and mechanical integrity, requiring a balance between productivity and weld quality. At 25 cm/min, higher heat input and slow cooling result in stronger, more ductile welds, but at the cost of reduced productivity. In contrast, 100-125 cm/min leads to rapid cooling, creating fine microstructures but increasing porosity and cracks, reducing tensile strength and deformability.The optimal speed of 60 cm/min balances mechanical properties and efficiency, making it ideal for industrial applications. These results provide guidance for optimizing welding parameters, improving the quality and performance of welded components in the pressure vessel industry.

R E F E R E N C E S

[1] S. Li, X. Yang, Y. Jiang, Influence of welding parameters on microstructure and mechanical properties of submerged arc welded P355N steel, Mater. Sci. Eng. A, Vol. **703**, 2017, pp. 394–402, DOI: 10.1016/j.msea.2017.07.029.

[2] J. Wang, X. Li, H. Liu, Microstructural evolution and mechanical properties of submerged arc welded P355N pressure vessel steel, Mater. Charact., Vol. **134**, 2018, pp. 57–64, DOI: 10.1016/j.matchar.2017.10.021.

[3] A. Sharma, P. Gupta, Investigation of the effect of welding speed on the mechanical properties of pressure vessel steel P355N by submerged arc welding, J. Manuf. Process., Vol. **56**, 2020, pp. 832–839, DOI: 10.1016/j.jmapro.2020.04.037.

[4] J. Li, H. Zhang, Y. Wang, Effect of welding speed on the microstructure and mechanical properties of P355N steel in submerged arc welding, J. Mater. Process. Technol., Vol. **291**, 2021, Article No. 117007, DOI: 10.1016/j.jmatprotec.2021.117007.
[5] L. Wu, D. Chen, Q. Zhang, Microstructural characterization and mechanical performance of P355N steel welded by submerged arc welding at different speeds, Mater. Charact., Vol. **186**, 2023, Article No. 111782, DOI: 10.1016/j.matchar.2022.111782.
[6] V. Jain, K. Patel, Optimizing welding speed for enhanced mechanical properties in submerged arc welding of P355N pressure vessel steel, J. Manuf. Sci. Eng., Vol. 146, Iss. 2, 2024, Article No. 021005, DOI: 10.1115/1.4049207.
[7] European Standard EN 10027-1:2005, Designation systems for steels—Part 1: Steel names, European Committee for Standardization, Brussels, 2005.
[8] European Standard EN 10216-3:2003, Seamless steel tubes for pressure purposes. Technical delivery conditions alloy fine grain steel tubes, European Committee for Standardization, Brussels, 2003.
[9] ESAB, Technical Handbook: Submerged Arc Welding—Fluxes and Wires for Joining Non and Low-Alloyed Steels, Stainless Steels and Nickel-Base Alloys, ESAB, Gothenburg, Sweden, 2019.
[10] M. Bodea, Sudare și procedee conexe (Welding and related processes), UTPRESS, Cluj-Napoca, Romania, 2016, ISBN 978-606-737-143-7.
[11] F. Túsz, Tratat de sudură (Welding treatise), Publishing House Sudura, Timișoara, Romania, 2003.
[12] European Standard EN ISO 4063:2009, Welding and allied processes—Nomenclature of processes and reference numbers, European Committee for Standardization, Brussels, 2009.
[13] N. Murugan, V. Gunaraj, Prediction and control of weld bead geometry and shape relationships in submerged arc welding of pipes, J. Mater. Process. Technol., Vol. **168**, 2005, pp. 478–487, DOI: 10.1016/j.jmatprotec.2005.08.005.
[14] Standard BS EN 895:1995, Destructive tests on welds in metallic materials—Transverse tensile test, British Standards Institution, London, UK, 1995.
[15] W.D. Callister, D.G. Rethwisch, Materials Science and Engineering, Wiley, Hoboken, NJ, USA, 2010, ISBN 0470419970.
[16] G. Amza, G.M. Dumitru, V.O. Rândaşu, C.G. Amza, Tratat de tehnologia materialelor (Materials technology treatise), Editura Academiei Române, București, Romania, 2002.
[17] V. Suciu, M.V. Suciu, Studiul materialelor (Materials study), Fair Partners, București, Romania, 2008, ISBN 978-973-1877-01-3.
[18] Y.H. Zhao, Y.Z. Guo, Q. Wei, T.D. Topping, Influence of specimen dimensions and strain measurement methods on tensile stress–strain curves, Mater. Sci. Eng. A, Vol. **525**, 2009, pp. 68–77, DOI: 10.1016/j.msea.2009.05.073.